ARL-TR-9955 ● AUG 2024

Advancing Lithium-Ion Battery Technology through Development and Characterization of Volume-Accommodated Silicon Anodes

by Cody A Gonzalez, Benjamin D Gregory, Rebecca H Lima, Dat T Tran, and Jan L Allen

NOTICES

Disclaimers

The findings in this report are not to be construed as an official Department of the Army position unless so designated by other authorized documents.

Citation of manufacturer's or trade names does not constitute an official endorsement or approval of the use thereof.

Destroy this report when it is no longer needed. Do not return it to the originator.

ARL-TR-9955 ● AUG 2024

Advancing Lithium-Ion Battery Technology through Development and Characterization of Volume-Accommodated Silicon Anodes

Cody A Gonzalez, Benjamin D Gregory, and Rebecca H Lima
University of Texas at San Antonio

Dat T Tran and Jan L Allen
DEVCOM Army Research Laboratory

REPORT DOCUMENTATION PAGE

1. REPORT DATE	2. REPORT TYPE	3. DATES COVERED	
		START DATE	END DATE
August 2024	Technical Report	6/2/2024	8/08/2024

4. TITLE AND SUBTITLE
Advancing Lithium-Ion Battery Technology through Development and Characterization of Volume-Accommodated Silicon Anodes

5a. CONTRACT NUMBER	5b. GRANT NUMBER	5c. PROGRAM ELEMENT NUMBER
5d. PROJECT NUMBER W911NF-23-2-0238	**5e. TASK NUMBER**	**5f. WORK UNIT NUMBER**

6. AUTHOR(S)
Cody A Gonzalez, Benjamin D Gregory, Rebecca H Lima, Dat T Tran, and Jan L Allen

7. PERFORMING ORGANIZATION NAME(S) AND ADDRESS(ES)	8. PERFORMING ORGANIZATION REPORT NUMBER
DEVCOM Army Research Laboratory ATTN: FCDD-RLA-GD Adelphi, Maryland 20783	ARL-TR-9955

9. SPONSORING/MONITORING AGENCY NAME(S) AND ADDRESS(ES)	10. SPONSOR/MONITOR'S ACRONYM(S)	11. SPONSOR/MONITOR'S REPORT NUMBER(S)
Research Faculty Fellows Program Under Secretary of Defense for Research and Engineering	USRE	

12. DISTRIBUTION/AVAILABILITY STATEMENT
DISTRIBUTION STATEMENT A. Approved for public release: distribution unlimited.

13. SUPPLEMENTARY NOTES
ORCIDs: Dat T Tran, 0000-0003-0099-1206; Jan L Allen, 0000-0003-3353-1142

14. ABSTRACT
Lithium-ion batteries are a universal mechanism of energy storage in modern life; however, the simultaneous need for higher-capacity and stable electrodes remains a persistent challenge. This work explores the electrochemical and morphological characterization of volume expansion accommodated silicon (Si) lithium-ion batteries. While Si remains a promising electrode material due to its high capacity, the large volumetric expansion it undergoes during battery cycling represents a challenge to its practical adaptation. This report focuses on experimental development and testing of a Si composite lithium-ion battery that allows for volume accommodation of the Si volumetric expansion during charging through free deflection (or motion) of the battery. By harnessing the expansion of the Si composite electrode, higher capacity and higher cycling will be possible and make way for an actuator, or bending battery, that can do physical and electrochemical work. In multifunctionality, this allows batteries to do useful work through bending action while expending minimum charge due to internal resistance-based losses. These actuators could pave the way for higher-capacity batteries with applications for the Warfighter.

15. SUBJECT TERMS
Energy Sciences, self-actuated structures, self-powered robotics, lithium-ion batteries, actuators

16. SECURITY CLASSIFICATION OF:			17. LIMITATION OF ABSTRACT	18. NUMBER OF PAGES
a. REPORT	b. ABSTRACT	C. THIS PAGE		
UNCLASSIFIED	UNCLASSIFIED	UNCLASSIFIED	UU	28

19a. NAME OF RESPONSIBLE PERSON	19b. PHONE NUMBER *(Include area code)*
Jan L Allen	(301) 394-0291

STANDARD FORM 298 (REV. 5/2020)
Prescribed by ANSI Std. Z39.18

Contents

List of Figures

Acknowledgments

This work was supported by start-up funding from the University of Texas at San Antonio and through the DOD through the Under Secretary of Defense for Research and Engineering Research Faculty Fellows Program. Support from the US Army Combat Capabilities Development Command (DEVCOM) Army Research Laboratory (ARL) Research Associateship Program is made possible through Oak Ridge Associated Universities for ARL through cooperative agreement W911NF-23-2-0238. We greatly appreciate Drs Jan Allen and Dat Tran for their guidance and collaboration.

1. Introduction

The work conducted in this report focuses on the development of silicon (Si)-composite-based lithium (Li)-ion battery actuators. It has been proven that Li-ion batteries can cause self-bending due to increased state of charge, but their ability to cycle reliability has proven difficult to overcome. Although electrochemical actuators are relatively slow due to their reliance on diffusion mechanisms, they remain an area of interest due to their strong potential for cyclability, self-powered nature, and high energy density capabilities. The aim is to better understand the effect of electrode composition on the battery self-powered bending and specifically to determine whether Si microparticles can be adapted for use in electrochemical actuators as a replacement for nanoparticles.

1.1 Actuator State of the Art

Mechanical actuators are defined by their ability to provide a driving force and motion, typically in response to a control signal. Huber et al.[1] present the performance indices of mechanical actuators, expressed in terms of force, displacement, stiffness, size, mass, response time, power, efficiency, and resolution. Some of the key performance characteristics of mechanical actuators include the maximum actuation stress σ_{max} and maximum actuation strain ϵ_{max}. Additionally, actuation strain is defined by the extension of an actuator of initial length L to a total length of $(1 + \epsilon)L$. Actuation stress is defined as the applied force per unit cross-sectional area. Some additional metrics, often used for cantilever-based actuators, are free deflection δ_z (i.e., the largest tip deflection of a cantilever beam under no loading) and the blocking force F_b, (i.e., the force required to achieve no transverse tip loading). Other metrics that complement these are the blocked deflection (i.e., the deflection along the cantilever length that results from applying a blocking force at the tip) and actuation force F_a (i.e., the force required to achieve a prescribed tip displacement). Work has been conducted in the past to measure the free deflection or Li-ion battery electrochemical actuators due to their strong potential for these performance characteristics and metrics.[2]

Li-ion batteries have a strong application for reversible actuators with high energy density.[3,4] Graphite has been explored extensively for its high cyclability and stability, but also for its potential for actuation.[4] For example, Koyama et al.[3] have estimated the theoretical energy density of multiple electrode materials to include graphite and Si. A 10% free strain has been found upon full lithiation.[5–7] Assuming a 10% free strain for graphite upon full lithiation and a Young's modulus E of 35 GPa in the [001] direction, the area under the stress–strain curve would be the product of the stress and strain. Koyama et al. adapt the figure from Huber et al. and

include their graphite microactuators and the tests they ran on high density composite electrodes, as shown in Fig. 1.

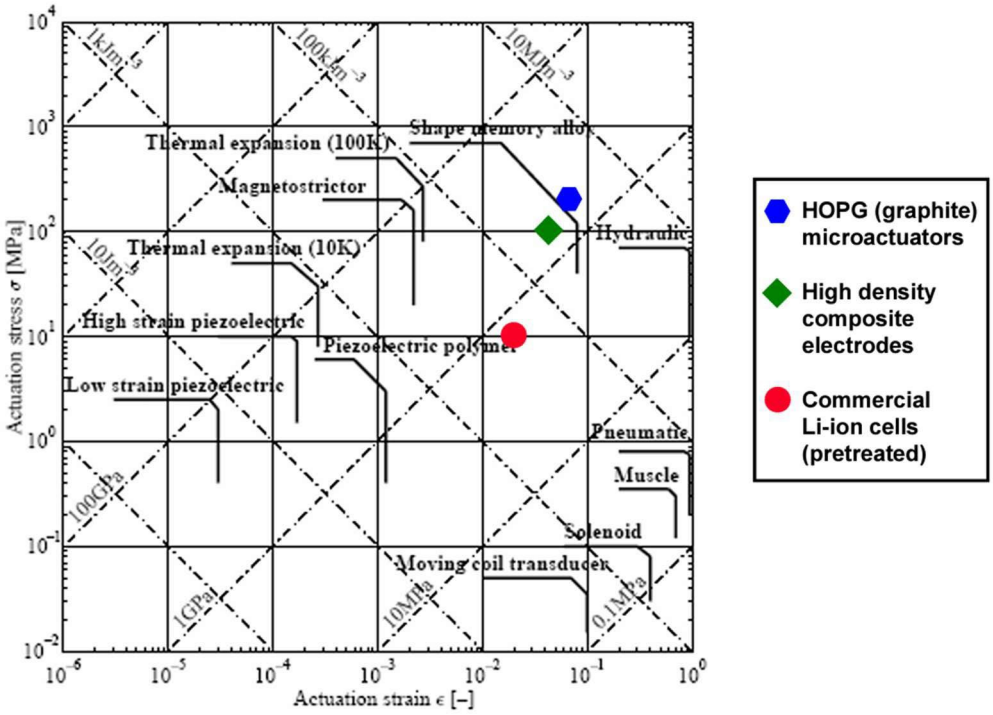

Fig. 1 Actuation stress, σ, vs. actuation strain, ϵ, for various actuators including Li-ion battery-based actuators[1,3]

Furthermore, according to density functional theory by Qi et al.,[8] the polycrystalline Young's modulus of graphite also triples when it is lithiated to LiC_6. However, Qi and Harris[9] also experimentally validated the findings for an increase in Young's modulus of lithiated graphite through observation that a graphite composite film is sufficiently porous to accommodate the approximately 10% free strain of graphite during lithiation.

However, some limiting factor of the performance of graphitic electrochemical actuators is their reliance on compliant plastic separators and on liquid electrolytes. Koyama et al.[3] recommended the inclusion of high-stiffness, load-bearing separators to increase actuator energy density.

1.2 Different Binders and N/P Ratios

There are many binders available for binding a Si composite coating, including polyacrylic acid (PAA) and carboxymethyl cellulose (CMC).[10,11] Generally, PAA is more efficient than CMC at higher binder percentages and PAA exhibits more flexibility as a bulk property that is desirable for the large expansion of Si anodes. Such "conductive glue" (CG) binders also have demonstrated success with high

areal capacity 5.13 $mAcm^2$ and high rate capacity 8400 mAg^{-1}.12 Si composite electrodes utilizing CG have shown a high cyclability of 1500 $mAhg^{-1}$ for over 700 cycles with a lower elastic modulus than PAA, CMC, polyvinylidene fluoride, polysaccharide/alginate, and poly(3,4-ethylenedioxythiophene): polystyrene sulfonate (PEDOT:PSS). As a cross-linked mixture of vinyl acrylic acetate ester copolymer, D-sorbitol, and PEDOT:PSS, the CG can be stretched up to 400% in volume without conductivity loss and mechanical failure. Other naturally derived binders such as polysaccharide (extracted from brown algae) forms a stable half-cell with Li but has a high elastic modulus averaging around 4.5 GPa. While highly stable in a half-cell, the rigidity of the binder would not be well-suited for the flexibility required of an actuator.[13]

While half-cells are often studied for cathode and anode separately, the Li insertion in full cells is also of importance, as the supply of Li is limited to the amount the cathode can provide. Chen et al.[14] studied the effect of N/P ratios on LiNCA||SiOx/graphite pouch cells and for a study of N/P ratios from 0.8 to 1.8, they find that a value close to unity is effective. N/P ratios are defined as the capacity of the anode or negative electrode (N) relative to the cathode or positive electrode (P). Commercial ratios of approximately 1.1 are used where there is more hosting capacity of Li in the negative electrode than Li donating capacity in the positive electrode.

However, to achieve this ratio commercially, graphite anodes are made larger than the cathodes to prevent Li plating on the bare current collector. O'Brien et al.[15] found that while an overhang (i.e., when one electrode is wider or longer than the other) in graphite-based Li-ion batteries homogenizes over time, Si-based batteries do not homogenize as quickly. Obrovac and Christensen[16] have noted that while $Li_{21}Si_5$ (or formerly, $Li_{22}Si_5$) may form, it is not the fully lithiated form of Si at room temperature. Instead, they report $Li_{15}Si_4$ as the final phase of lithiation at room temperature, dropping the expected reversible capacity from approximately 4008 $mAhg^{-1}$ (or 4200 $mAhg^{-1}$) to about 3500 $mAhg^{-1}$ at room temperature. Similarly, Hasa and Passerini[17] reviewed the state of the art for Si anodes, mentioning that Li15Si4 is the final state of lithiation at room temperature, and that Li22Si5 has been observed only by X-ray diffraction after holding the cell potential at 0 V for 24 h.[18]

While the final state of lithiation is a matter of contention, it has been proven for both graphite and Si that electrode materials increase in Young's moduli with increasing states of lithiation.[8,19,20] Ratchford et al. found that for both phases of $Li_{12}Si_7$ and $Li_{22}Si_5$, the elastic moduli changes relative to unlithiated Si—52 GPa and 35.4 GPa, respectively. While graphite has a threefold increase in Young's moduli due to lithiation, Si becomes more compliant with increasing lithiation from

173 GPa (nanoindentation of Si thin films) down to 35.4 GPa for $Li_{22}Si_5$. Future modeling should take this change in elasticity of Si films into account, as it may be a mechanism for failure that prevents adoption of graphite-based coating binding materials.

2. Experimental

The goal of this work is to reproduce previous work by Ma et al.[21] and extend its suitability for adoption by replacing Si nanoparticles, which are typically expensive, with Si microparticles.

2.1 Silicon Composite Anodes

Current work is being undertaken on the use of 10-μm Si microparticles with an appropriate mixture of conductive and binding agents. Zhang[11] found that the content and type of binders has a strong effect on Si composite anodes. He tested both PAA and CMC and found that an optimal binder content falls between 20 wt% and 25 wt%.[11]

Following the recipe implemented by Zhang,[11] a 60:15:25 ratio of active, conductive, and binding agent was used to tape cast a Si composite anode with a doctor blade. Starting with an active ingredient weight of 0.1 g, a 4:1 ratio of active to conductive agent and a 3:1 ratio of combined active and conductive agents to total binder were maintained with a 6.5% solid-to-liquid wt%. However, further testing with an alternate conductive agent required a higher solid-to-liquid wt% and alternate ratio.

Microsized Si particles (Si-MP, with D90 of 10.0 ± 1.0 μm) and CMC powder were purchased from MSE Supplies LLC and used as received. A 25% PAA aqueous solution was purchased from Alfa Aesar and ketjenblack (EC300J) was purchased from Akzo Nobel Chemicals Inc. The CMC powder was dissolved in deionized water to form a 2% solution. The 3% solution presented difficulty in pipetting due to its high viscosity. The Si electrodes are coated by mixing the Si powder and conductive agent (ketjenblack) in varying ratios of 75:5, 72.5:7.5, 70:10, and by first adding them into a 7-mL polypropylene (PP) vial and shaking with a 6-mm-diameter stainless-steel ball at 2000 rpm for 2 min on a 5120 Mixer/Mill mixer (SPEX SamplePrep).

After the dry ingredients are mixed, a consistent (4:1; active and conductive binder) 85:15 mixture of PAA and CMC was added with deionized water until a fixed solid content (~25%) was reached. The complete slurry was then shaken for an additional 10 min, followed by coating onto a copper foil via doctor blade and allowed to

evaporate into the air, followed by being vacuum-dried at 110 °C under vacuum overnight. After drying, the Si electrode was punched into discs with a diameter of 12.7 mm. Si loading for the 5%, 7.5%, and 10% ketjenblack was 2.12, 0.79, and 2.46 $mgcm^{-2}$, respectively. Assuming a theoretical capacity of 4200 $mAhg^{-1}$ for the Si microparticles, the C-rate was calculated with a respective 1C rate of 0.00418 Amg^{-1}.

The electrolyte used was a commercial solution of 1.0 M $LiPF_6$ dissolved in a 10:45:45 (wt%) mixture of fluorinated ethylene carbonate, ethylene carbonate, and diethyl carbonate. In a dry room, CR2032-type Li/Si coin cell were assembled with a disc of Celgard 2340 separator and filled with a fixed amount (100 μL) of electrolyte. The cells were sealed with an automatic coin cell crimper (HSACC-10; Hohsen Corp) and cycled on a Maccor Series 4000 cycler.

2.2 Optimizing Electrode Composition by Altering Conductive Agent

Upon exploration of other conductive agents, ketjenblack was found to give a higher surface area as a conductive agent that could improve the conductivity while allowing for a reduction in conductive and binding agent. By implementing this in a fixed ratio of 4:1 active and conductive agent to binding agent, a preferred percentage of ketjenblack was found that allowed for a reasonable high-cyclability Si anode using 10-μm-diameter average Si microparticles.

The discharge capacity of 10-μm Si microparticles in a composite matrix of ketjen black and a mixed binder consisting of 85% PAA and 15% CMC for balanced cyclability and coating viscosity is shown in Fig. 2. The CR2032 half-cells (Si/Li) were discharged (lithiation of Si) at a constant C/10 rate (C representing the full charge of Si at 4200 $mAhg^{-1}$) until 0.05 V, then held at 0.05 V until the current dropped to C/50 or the elapsed time exceeded 3 h (constant current constant voltage [CCCV] cycling). After discharge, the cell was then charged (delithiation of Si) at a constant C/10 rate until the voltage exceeded 1.25 V. After two formation cycles, the battery was then discharged at C/2 (CCCV) and charged at C/2 constant current. The lack of consistent CCCV on both charge and discharge cycles contributes to the inconsistent coulombic efficiencies and anomalous residual capacity shown in Figs. 3 and 4, respectively. Columbic efficiency *CE* is defined as a metric to gauge internal reactions that affect battery life where the discharge capacity of cycle n, $C_{Dch(n)}$ is divided by the measured charge capacity $C_{Ch(n)}$:

$$CE = \frac{C_{Dch(n)}}{C_{Ch(n)}}. \quad (1)$$

However, the residual capacity RC, or effectively the cumulative columbic efficiency, is defined here as the amount of total capacity remaining as a function of the ith cycle number up to n:

$$RC = \sum_{i=1}^{n} \frac{C_{Dch(i)}}{C_{Ch(i)}}. \quad (2)$$

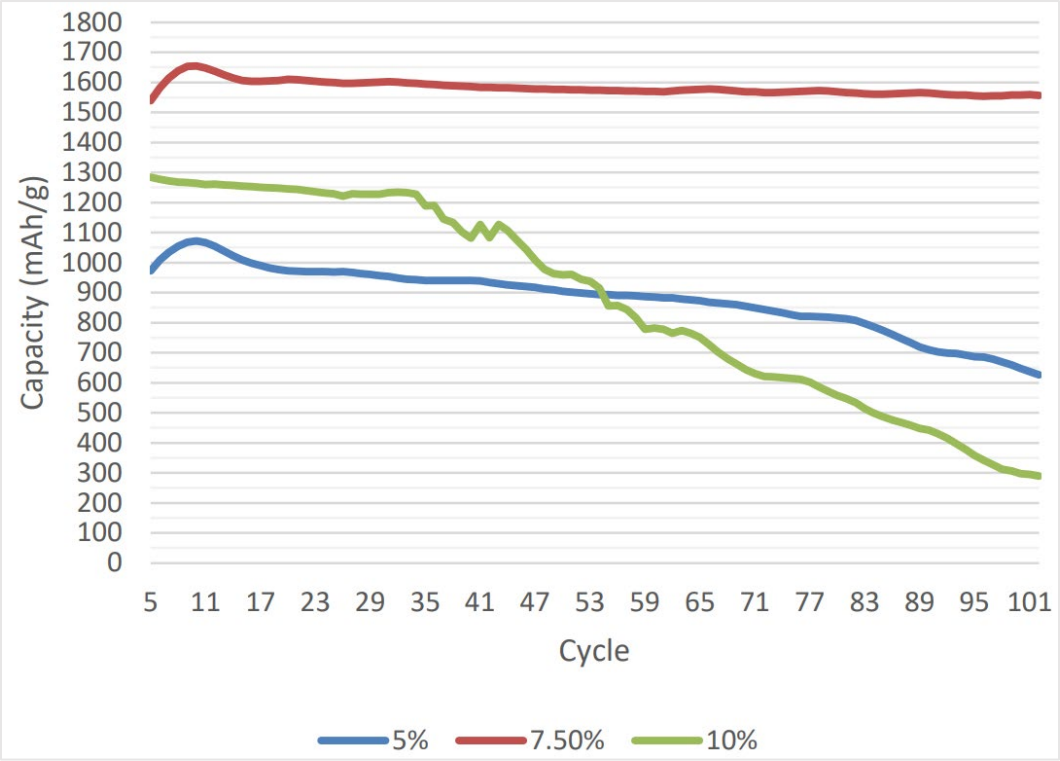

Fig. 2 Specific capacity (mAhg^{-1}) vs. cycle number for increasing percentages of conductive agent ketjenblack

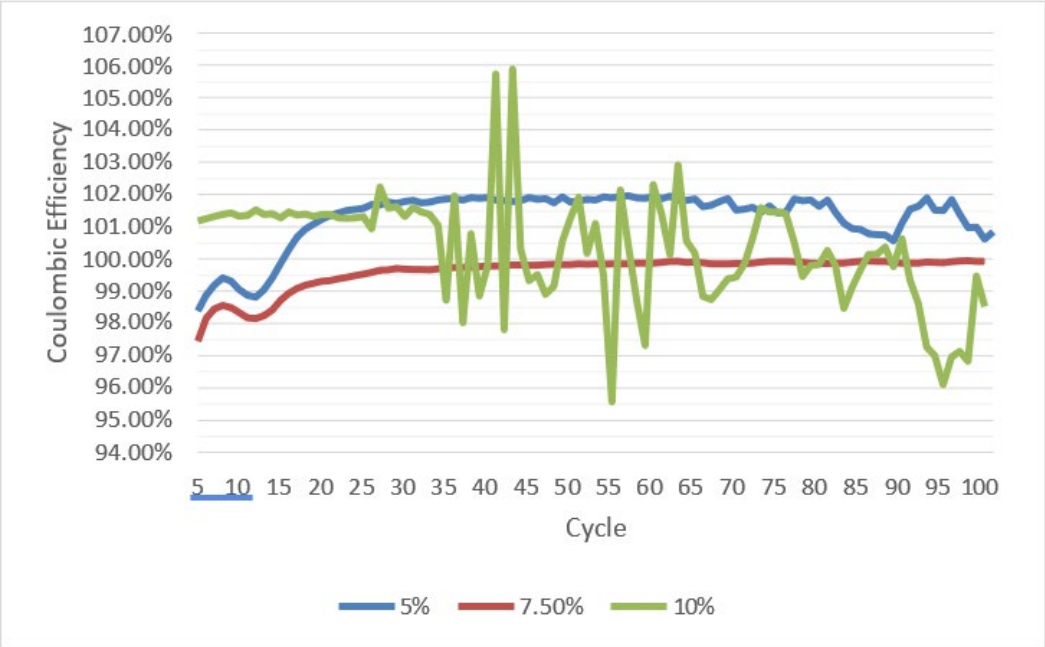

Fig. 3 Coulombic efficiency (%) vs. cycle number for increasing percentages of conductive agent ketjenblack

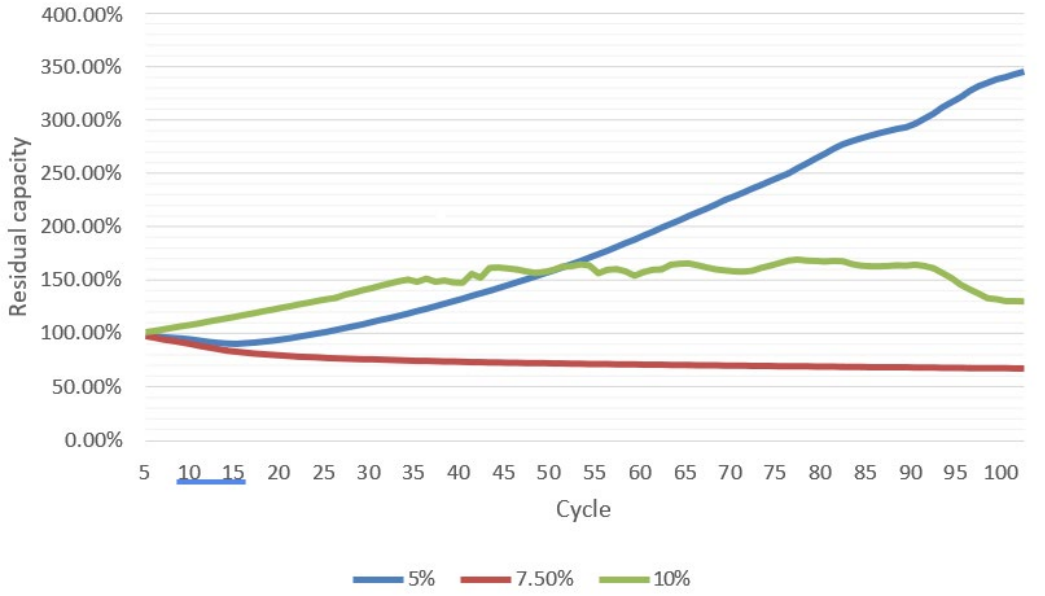

Fig. 4 Residual capacity vs. cycle number for increasing percentages of conductive agent ketjenblack

However, the cycling data for the 72.5:7.5:20 (7.5% ketjenblack) composition appears to cycle well and the half-cell maintains a specific capacity of 1550 $mAhg^{-1}$ with the use of 10-µm Si microparticles. Due to the high porosity of ketjenblack, an optimal ratio of 7.5% relative to binder and active material creates

a highly cyclable anode. Additional studies of higher percentages of ketjenblack in a 6:2:2 or 60:15:25 compositions did not cycle as well because of the higher occupation of the binding agents by ketjenblack instead of the active Si. Due to the upper voltage limit of 1.25 V, the maximum state of charge is limited along with the volume expansion. This limitation enables the relatively high cyclability of Si microparticles (hundreds of cycles). While Zhang[11] calculated charging rate based on 2000 $mAhg^{-1}$ with a voltage window from 0.005 to 1 V, this work used a charging rate based on 4200 $mAhg^{-1}$ with a voltage window from 0.05 to 1.25 V, effectively increasing the relative C-rate to 1C while capturing similar specific capacity after 100 cycles (~1700 $mAhg^{-1}$) to our 1550 $mAhg^{-1}$. A 72.5% active Si is used, compared with their approximately 64% active Si (for a 4:1 weight ratio of active to conductive agents with a 3:1 ratio for conductive and active agents to binder). Future studies would benefit from consistent CCCV charge and discharge cycling.

2.3 Chamber Design and Experimental Setup

To conduct experiments involving the real-time deflection of Si composite anodes, an experimental chamber was developed to extend on previous work.[21–23] As shown in Fig. 5, the experimental chamber was created by both milling and additive manufacturing. The blue external front clamp and orange back clamp, shown in the expanded view Fig. 6, were 3D printed out of polylactic acid (PLA) with a high percentage infill and clamped around a PP chamber that was created on a mill and lathe. While PLA is not inert to the organic solvents used, PP is and thus was used for the next containment. The viewing pane is made from thick borosilicate glass. However, to reduce the amount of electrolyte needed for testing, a standard polyacrylic slide was used with the plastic “electrolyte mount” with the 1-cm scale mark and sealed with silicone sealant. The wires are routed through the top of the chamber, as shown in Fig. 6.

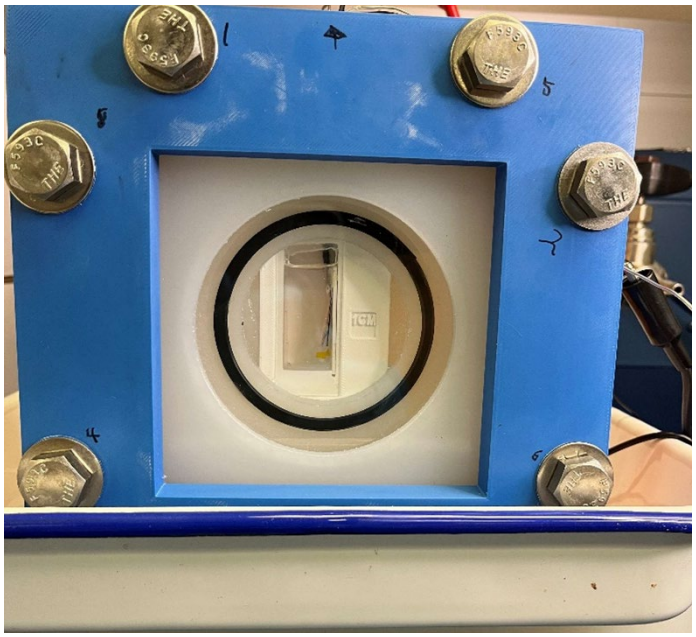

Fig. 5 An experimental chamber was developed with a self-contained insert for observation of the electrode deformation while cycling (front view)

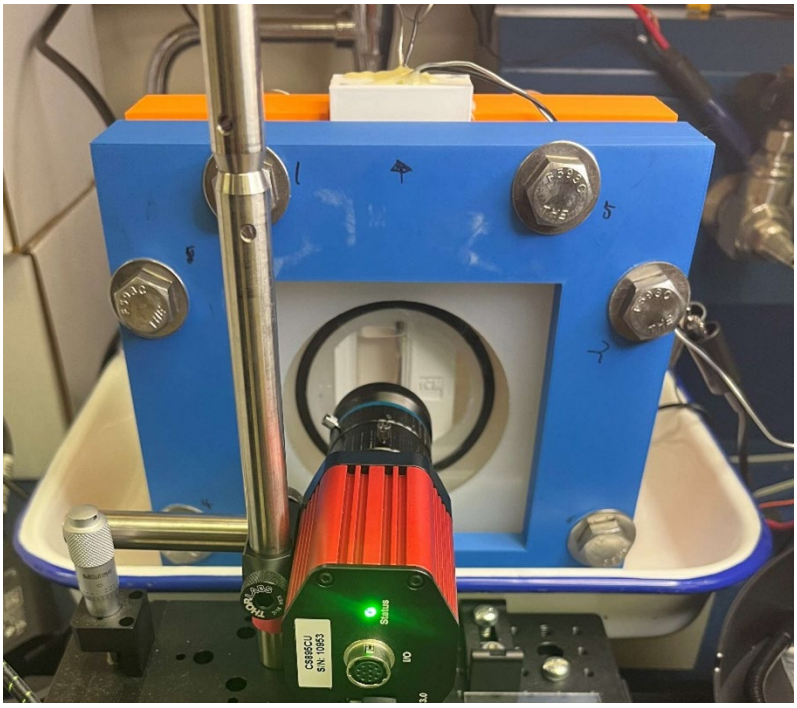

Fig. 6 The deflection was captured in real time by video or by routine capture of images once every minute for the duration of cycling

Following the requirement to utilize less electrolyte, Chamber 4-1 was altered to accompany an insert. This Electrolyte Mount 4-1 originally sat inside Chamber 4-1 without alterations (Fig. 7). This design used 20 mL of electrolyte

versus 127 mL for the chamber without the insert. Prototypes were created out of acrylonitrile butane styrene (ABS) plastic and tested for electrolyte compatibility, where it was discovered that ABS reacts with the electrolyte, rendering it unusable for future tests. Filaments made from PP, polyethylene terephthalate glycol (PET-G), and thermoplastic polyurethane (TPU) were sourced as a replacement. PP filament showed the best chemical properties but would cause damage to the 3D printer during an attempt to print a test chamber.

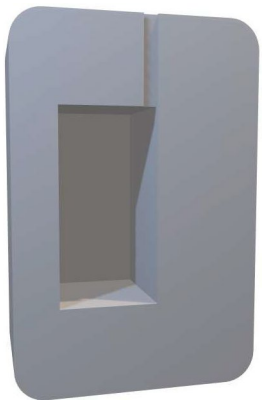

Fig. 7 Electrolyte Mount 4-1

TPU worked with the printer but absorbed the electrolyte during a test run, rendering it unsuitable for use. PET-G was the least compliant of the three choices, requiring the nozzle of the printer to be cleaned after each use. However, it provided the required chemical properties for the tests, so it was selected for the chamber designs.

Electrolyte Mount 4-1 allowed for a reduction in electrolyte usage but did not provide a way to mount wiring. To solve this issue, Chamber 4-1 would be altered into Chamber 4-2, as shown in Fig. 8. This alteration would allow for a larger electrolyte mount, which would be easier to insert into the chamber and be able to accommodate holes for the copper and aluminum wiring.

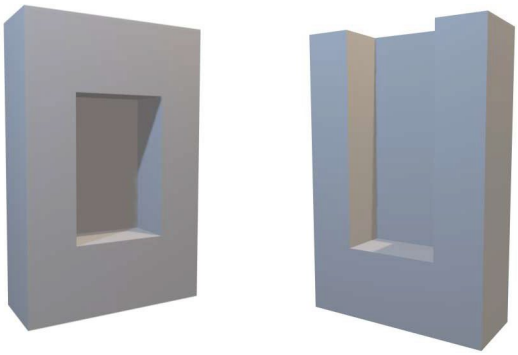

Fig. 8 Chamber 4-1 (left) to Chamber 4-2 (right)

Electrolyte Mount 4-2 would keep the same inner dimensions as 4-1 but increase the length of the chamber, adding a hole for wires and handle to remove the insert from the chamber. The handle on Electrolyte Mount 4-2 would prove difficult to print, and the wires could not fit easily through the hole in the chamber (Fig. 9). Attaching the electrodes to the walls of the chamber also proved to be difficult without warping the electrodes. Electrolyte Mount 4-3 would solve these issues by removing the handle and making the chamber longer, as well as increasing the size of the hole and making it square to simplify the printing geometry (Fig. 10). A second hole was added to allow for two simultaneous tests, and a separate electrolyte filling port was also added. The chamber's height was increased to 50 mm to provide room for the wires inside the chamber. To allow for the electrodes to be mounted, another internal mount was created (called the matryoshka piece), which the electrodes would be attached to prior to mounting inside the electrolyte mount. A 1-cm square marker also was added to allow for pixel counting in postprocessing studies.

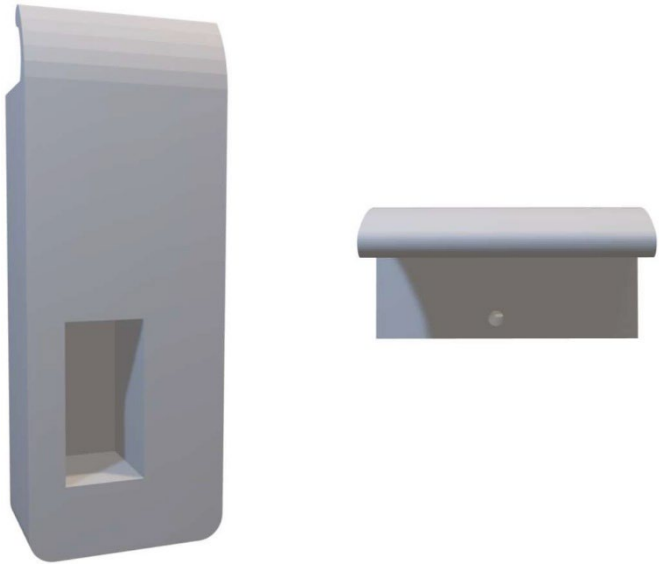

Fig. 9 Electrolyte Mount 4-2, featuring a handle and a hole for wires

Fig. 10 Electrolyte Mount 4-3 (left); top view (middle); matryoshka piece (right)

2.4 Electrochemical Actuator Testing

With a 3D-printable PET-G chamber insert electrolyte mount created effectively, in situ testing of the Li-ion battery actuators could begin. Figure 11 shows the first two formation cycles of the Si microparticle-based electrochemical actuators. The nickel manganese cobalt (5:3:2) cathode purchased from MTI was mounted against the rightmost wall of the electrolyte mount piece in a Celgard 2340 separator pouch. The anodes are shown deflecting and had some initial deformation in addition to swelling that occurred when the electrolyte penetrated the Si composite coating (shown in Fig. 11a). With an actuator beam length of approximately 2.5 cm long and 4 mm wide, the anode achieved approximately 1 cm of deflection to the left or approximately 40% tip deflection upon the first lithiation of Si (Fig. 11b).

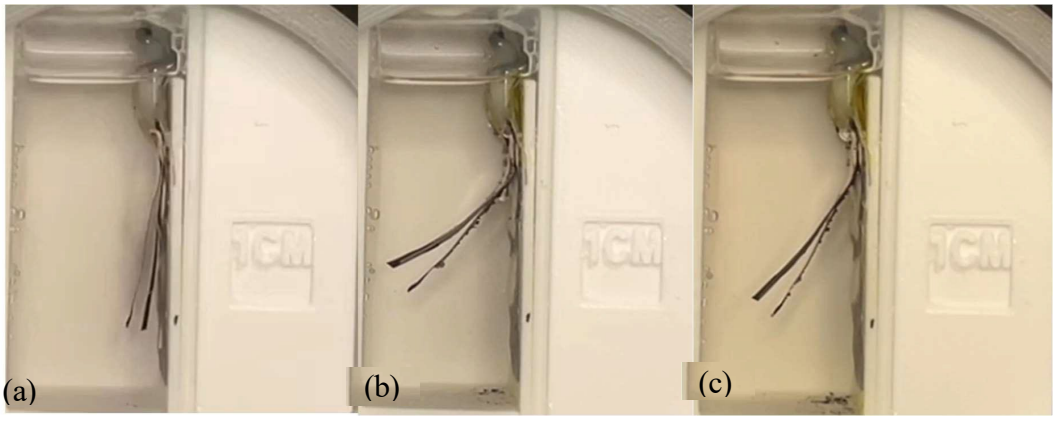

Fig. 11 In situ lithiation of a Si composite anode electrochemical actuator (a) precycle 1; (b) postcycle 1; (c) postcycle 2

However, after two complete formation cycles at an initially estimated C/10 rate, the electrode exhibited a poor deflection hysteresis, as shown in Fig. 11c. The fail to recovery back to the starting position is thought to be due to a few possible causes including permanent deformation of the copper foil current collector, irreversible capacity loss of the Si and delamination of the coating from the current collector, and Si expansion filling the pores in the porous coating layer. The initial capacity was overestimated so that two cycles at C/10 that should have lasted approximately 40 h lasted only 4 h. By re-estimating the capacity based on the duration of charge, it is estimated that the initial cycling was at near 1C, ten times the intended cycling rate for formation. This overestimation of capacity was assumed to be due to a combination of difficulty getting precise measurements of active mass and an overestimation of the max capacity of the electrodes. Future tests will be conducted with a lower charging rate.

Both the percent residual capacity and voltage curve agree with this unexpectedly increased charging rate. After the initial approximately 1C rate (formerly C/10), then the electrodes are cycled at 5C (formerly C/2), which led to near-instant capacity fade and a very low residual capacity, as shown in Fig. 12. With the total cycling time of two formation cycles at approximately 10 h, as shown in Fig. 13, it seems that the large capacity loss may be partially due to a quicker cycling time.

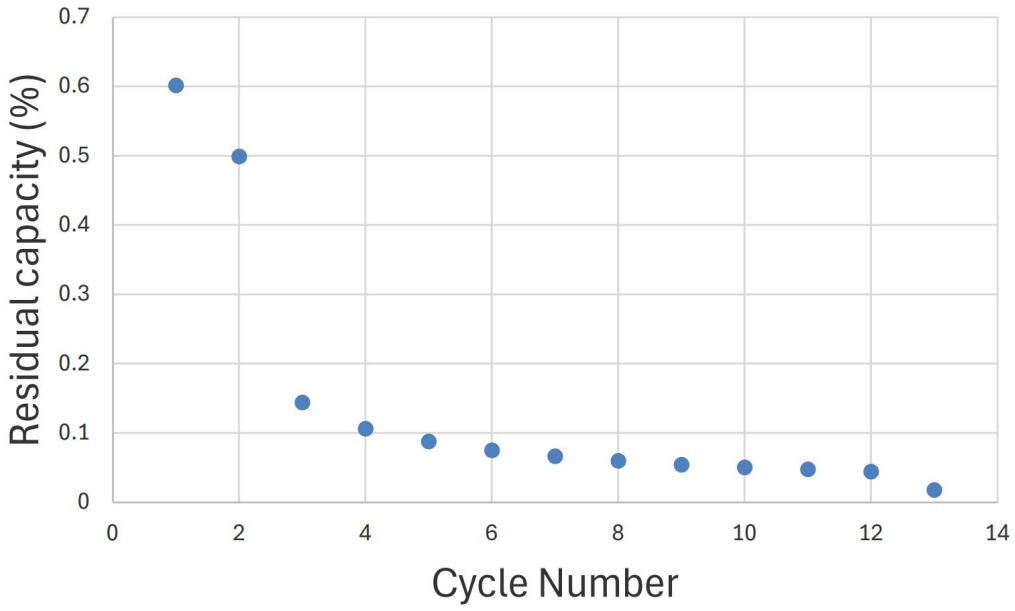

Fig. 12 Residual capacity of a Si composite anode electrochemical actuator vs. cycling

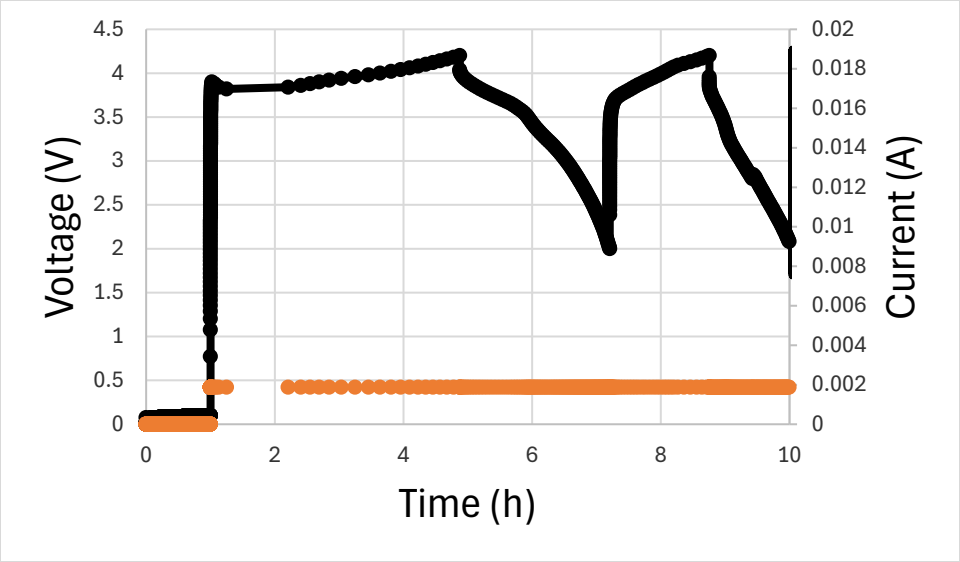

Fig. 13 Voltage profile of an electrochemical actuator vs. time for two formation cycles

3. Conclusion

The work achieved its primary goal of achieving electrochemical actuation using Si microparticles, thus advancing the state of the art of Si-based electrochemical actuators from their reliance on Si nanoparticles. Reliable cycling of the actuators remains an issue, and future work proposes the use of more compliant polymer-based electrodes and further optimization of the current collector-coating layer interface. Additionally, changing the mode of actuation from bending to out-of-plane actuation is attractive in its reliance on testing the actuator under a compressive load. By keeping the Si compressed, as it would be during the relatively stable cycling Si/Li half-cells shown, the actuators are more stable and higher performing.

4. References

1. Huber JE, Fleck NA, Ashby MF. The selection of mechanical actuators based on performance indices. Proc R Soc Lond Ser Math Phys Eng Sci. 1997;453(1965). http://doi.org/10.1098/rspa.1997.0117.

2. Gonzalez CA, Shan S, Frecker MI, Rahn CD. Analytical modeling of a multilayer, multimorph lithium-ion battery actuator. J Intell Mater Syst Struct. 2023;34(12). http://doi.org/10.1177/1045389X221136540.

3. Koyama Y, Chin TE, Rhyner U, Holman RK, Hall SR, Chiang Y-M. Harnessing the actuation potential of solid-state intercalation compounds. Adv Funct Mater. 2006;16(4):492–498. http://doi.org/10.1002/adfm.200500633.

4. Chin TE, Rhyner U, Koyama Y, Hall SR, Chiang Y-M. Lithium rechargeable batteries as electromechanical actuators. Electrochem Solid-State Lett. 2006;9(3):A134. http://doi.org/10.1149/1.2161523.

5. Kohanoff J, Galli G, Parrinello M. Theoretical study of LiC 6. J Phys IV. 1991;01(C5): C5-351–C5-356. http://doi.org/10.1051/jp4:1991541.

6. Fischer JE, Fuerst CD, Woo KC. Staging transitions in intercalated graphite. Synth Met. 1983;7(1–2):1–12. http://doi.org/10.1016/0379-6779(83)90076-0.

7. Xu Z, Shi X, Zhuang X, Wang Z, Sun S, Li K, Zhang T-Y. Chemical strain of graphite-based anode during lithiation and delithiation at various temperatures. Research. 2021;2021:9842391. http://doi.org/10.34133/2021/9842391.

8. Qi Y, Guo H, Hector LG, Timmons A. Threefold increase in the Young's Modulus of graphite negative electrode during lithium intercalation. J Electrochem Soc. 2010;157(5):A558. http://doi.org/10.1149/1.3327913.

9. Qi Y, Harris SJ. In situ observation of strains during lithiation of a graphite electrode. J Electrochem Soc. 2010;157(6):A741. http://doi.org/10.1149/1.3377130.

10. Karkar Z, Guyomard D, Roué L, Lestriez B. A comparative study of polyacrylic acid (PAA) and carboxymethyl cellulose (CMC) binders for Si-based electrodes. Electrochimica Acta. 2017;258:453–466. http://doi.org/10.1016/j.electacta.2017.11.082.

11. Zhang SS. Effect of the content and type of binders on electrochemical performance of silicon anode materials. Chem Phys Chem. 2024:e202400570. http://doi.org/10.1002/cphc.202400570.

12. Wang L, Liu T, Peng X, Zeng W, Jin Z, Tian W, Gao B, Zhou Y, Chu PK, Huo K. Highly stretchable conductive glue for high-performance silicon anodes in advanced lithium-ion batteries. Adv Funct Mater. 2018;28(3):1704858. http://doi.org/10.1002/adfm.201704858.

13. Kovalenko I, Zdyrko B, Magasinski A, Hertzberg B, Milicev Z, Burtovyy R, Luzinov I, Yushin G. A major constituent of brown algae for use in high-capacity li- ion batteries. Science. 2011;334(6052):75–79. http://doi.org/10.1126/science.1209150.

14. Chen Z, Zhang L, Wu X, Song K, Ren B, Li T, Zhang S. Effect of N/P ratios on the performance of LiNi0.8Co0.15Al0.05O2||SiOx/Graphite lithium-ion batteries. J Power Sources. 2019;439:227056. http://doi.org/ 10.1016/j.jpowsour.2019.227056.

15. O'Brien AI, Trask SE, Salpekar D, Son S-B, Dunlop AR, Veith GM, Lu W, Ingram BJ, Abraham DP, Jansen AN, et al. Inactive overhang in silicon anodes. J Electrochem Soc. 2024;171(7):070519. http://doi.org/10.1149/1945-7111/ad5d22.

16. Obrovac MN, Christensen L. Structural changes in silicon anodes during lithium insertion/extraction. Electrochem Solid-State Lett. 2004;7(5):A93. http://doi.org/10.1149/1.1652421.

17. Hasa I, Passerini S. Chapter 1 - Silicon anode systems for lithium-ion batteries. Silicon anode systems for lithium-ion batteries. In: Kumta PN, Hepp AF, Datta MK, Velikokhatnyi OI, eds. Silicon anode systems for lithium-ion batteries Elsevier; 2022. p. 3–46. http://doi.org/10.1016/B978-0-12-819660-1.00002-5.

18. Kwon JY, Ryu JH, Oh SM. Performance of electrochemically generated Li21Si5 phase for lithium-ion batteries. Electrochimica Acta. 2010;55(27):8051–8055. http://doi.org/10.1016/j.electacta.2010.01.054.

19. Ratchford JB, Schuster BE, Crawford BA, Lundgren CA, Allen JL, Wolfenstine J. Young's modulus of polycrystalline Li22Si5. J Power Sources. 2011;196(18):7747–7749. http://doi.org/10.1016/j.jpowsour.2011.04.042.

20. Ratchford JB, Crawford BA, Wolfenstine J, Allen JL, Lundgren CA. Young's modulus of polycrystalline Li12Si7 using nanoindentation testing. J Power Sources. 2012;211:1–3. http://doi.org/10.1016/j.jpowsour.2012.02.027.

21. Ma J, Gonzalez C, Huang Q, Farese J, Rahn C, Frecker M, Wang D. Multifunctional Li(Ni0.5Co0.2Mn0.3) O2-Si batteries with self-actuation and self-sensing. J Intell Mater Syst Struct. 2020;31(6):860–868. http://doi.org/10.1177/1045389X19898768.

22. Ma J, Rahn CD, Wang D, Frecker MI, Thole KA. Multifunctional Li-ion battery: structures, actuators, and sensors [dissertation]. Pennsylvania State University; 2019. https://etda.libraries.psu.edu/catalog/16583jxm1153.

23. Shan S, Gonzalez C, Rahn C, Frecker M. Experimental study of NCM-Si batteries with bi-directional actuation. Proceedings of the ASME 2021 Conference on Smart Materials, Adaptive Structures and Intelligent Systems; 2021 Sep 14–15. American Society of Mechanical Engineers. http://doi.org/10.1115/SMASIS2021-67596.

Appendix A. Recording of Battery Actuation

A.1 Video 1

The test shown in the accompanying video* displays the large tip deflection that results from the charging of two silicon (Si) composite coated anodes connected by a nickel tab bus bar, which allows them to be held at the same potential bias. The video occurs over roughly 10 h and shows two formation cycles of actuation.

A.2 Video 2

The test shown in the accompanying video* displays tip deflection similar to that of video 1 and is similarly sped up; however, to improve the cyclability and lithium (Li) distribution along the length of the anode, the cathode is attached to the anode by a faux pouch cell made of heat-sealed separators. Kapton tape (in yellow) is attached to the tip of the separator for automated image postprocessing. About halfway through the video, a large slip occurs in one of the cells as the cathode slips and is brought back to its starting position. This experimentally validates previous modeling work that has shown how the ability of an electrochemical actuator to do work is highly dependent on its ability to be perfectly bonded and not slip.[1]

* Video clips are available as separate files from the report PDF.

[1] Gonzalez CA, Shan S, Frecker MI, Rahn CD. Analytical modeling of a multilayer, multimorph lithium-ion battery actuator. J Intell Mater Syst Struct. 2023;34(12). http://doi.org/10.1177/1045389X221136540.

List of Symbols, Abbreviations, and Acronyms

3D	three-dimensional
ABS	acrylonitrile butane styrene
ARL	Army Research Laboratory
CCCV	constant current constant voltage (cycling)
CG	conductive glue
CMC	carboxymethyl cellulose
DEVCOM	US Army Combat Capabilities Development Command
DOD	Department of Defense
Li	lithium
N/P	negative electrode/positive electrode
PAA	polyacrylic acid
PEDOT:PSS	poly(3,4-ethylenedioxythiophene): polystyrene sulfonate
PET-G	polyethylene terephthalate glycol
PLA	polylactic acid
PP	polypropylene
Si	silicon
TPU	thermoplastic polyurethane

1 (PDF)	DEFENSE TECHNICAL INFORMATION CTR DTIC OCA
1 (PDF)	DEVCOM ARL FCDD RLB CI TECH LIB